Supporting Information

Facile synthesis of defect-modified thin layered and porous g-C_3N_4 with synergetic improvement for photocatalytic H_2 production

Yanbin Huang [†, ‡, §], Jun Liu[†, ‡], Chao Zhao [‡], Xiaohao Jia [‡], Mengmeng Ma [‡], Yuanyuan Qian [‡], Cheng Yang [‡], Kong Liu [‡], Furui Tan[ǂ], Zhijie Wang[, ‡], Xiaobao Li[*, ‡, §], Shengchun Qu[*, ‡] and Zhanguo Wang [‡]*

[‡] Key Laboratory of Semiconductor Materials Science, Beijing Key Laboratory of Low Dimensional Semiconductor Materials and Devices, Institute of Semiconductors, Chinese Academy of Sciences, Beijing 100083 China; Center of Materials Science and Optoelectronics Engineering, University of Chinese Academy of Sciences, Beijing 100049, China.

[§]School of Mathematical Science and Engineering, Hebei University of Engineering, Handan 056038 China.

[ǂ] Key Laboratory of Photovoltaic Materials, Department of Physics and Electronics, Henan University, Kaifeng 475004, Henan, China.

[§] School of Civil Engineering, Hefei University of Technology, Hefei 230009 China.

[†] These authors contributed equally to this work.

[*] Corresponding authors.

E-mail addresses: wangzj@semi.ac.cn (Zhijie Wang), xiaobaoli@hfut.edu.cn (Xiaobao Li), qsc@semi.ac.cn (Shengchun Qu)

Figure S1. SEM images of (a) MCN-B, (b) MCN, (c) M_3U_1, (d) M_1U_1, (e) M_1U_2, (f) M_1U_3, (g) M_1U_4 and (h) 10KMCN.

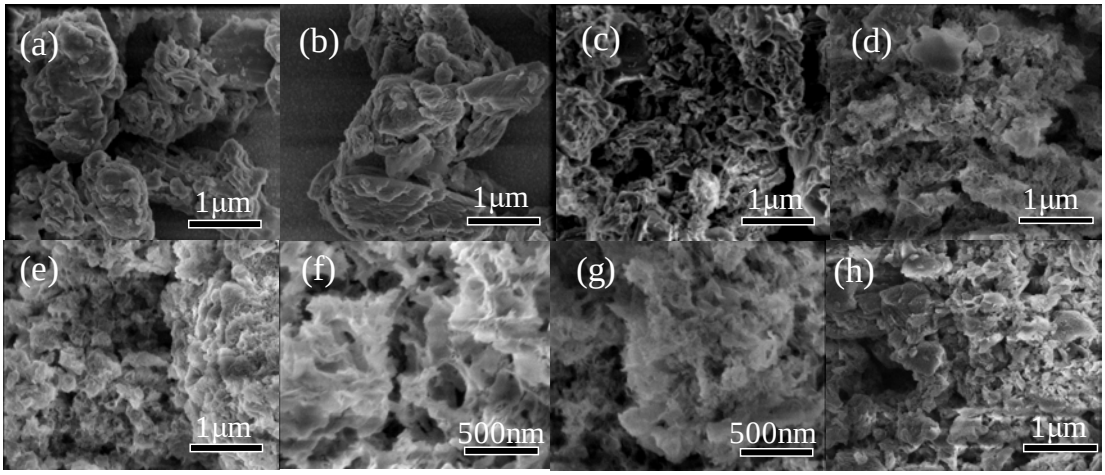

Figure S2. SEM images of (a) 1KCN, (b) 5KCN, (c) 10KCN, (d) 15KCN, (e) 20KCN, (f) 40KCN, (g) 100KCN and (h) 200KCN.

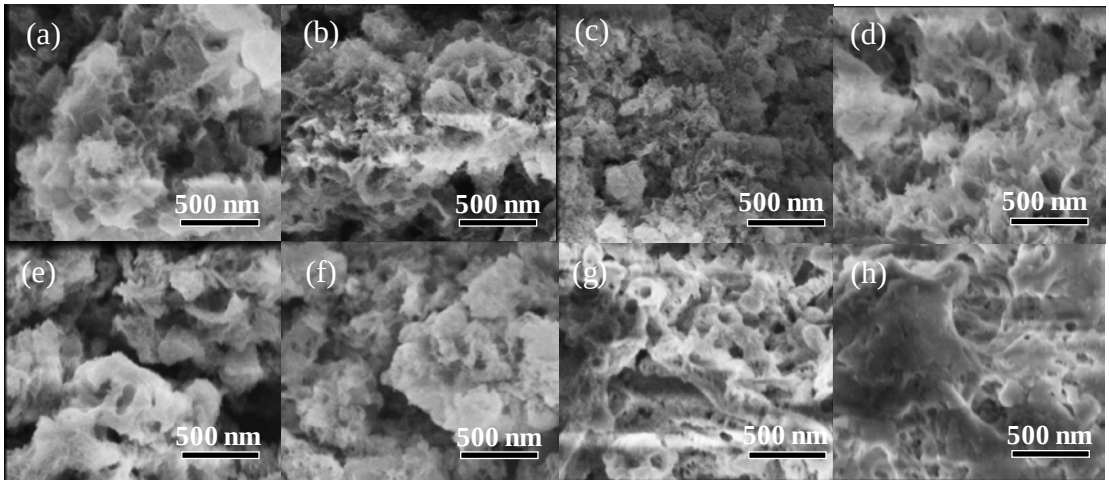

Figure S3. AFM images of (a) MCN-B, (b) MCN, (c) 10KMCN, (d) M_1U_3 and (e)10KCN.

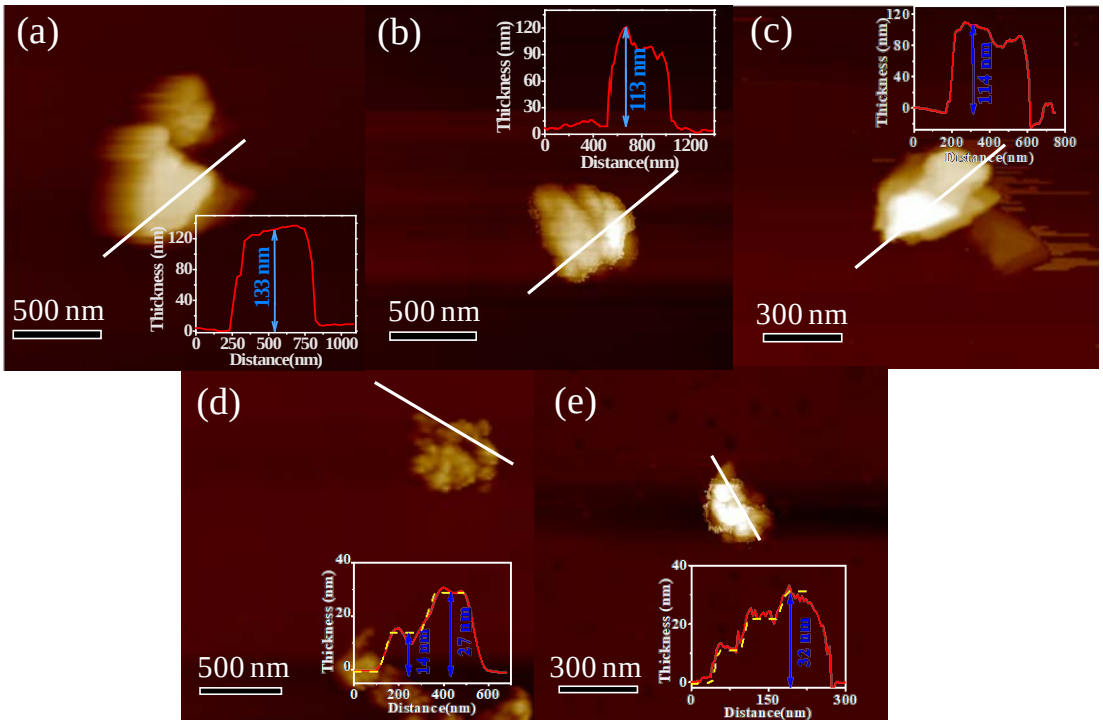

Figure S4. The HRTEM image of 10KCN.

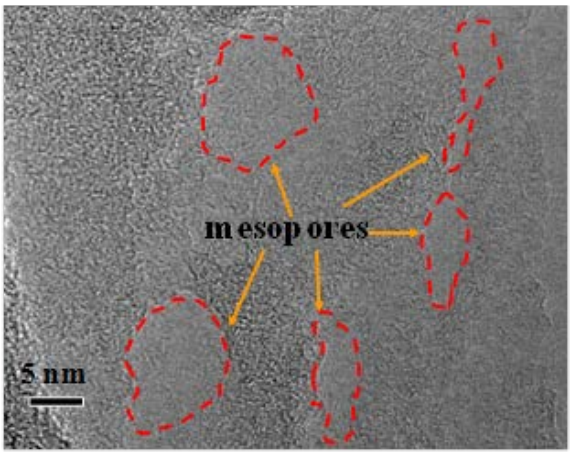

Figure S5. BJH pore size distribution of MCN-B, MCN, M_1U_3, M_1U_4, 10KCN and 10KMCN.

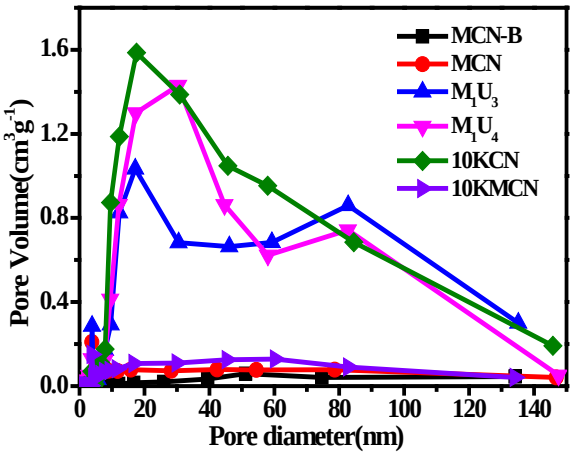

Table S1. Surface areas and pore parameters of MCN-B, MCN,10KMCN, M_1U_3, M_1U_4 and10KCN.

Sample	Surface area (m^2 g^{-1})	Pore volume (cm^3 g^{-1})	Average pore diameter (nm)
MCN-B	6.104	0.0429	3.805
MCN	26.565	0.1206	3.778
10KMCN	28.727	0.1439	3.782
M_1U_3	123.84	0.8837	3.853
M_1U_4	180.457	1.104	17.346
10KCN	199.394	1.306	12.276

Figure S6. XRD patterns of (a) MCN-B, MCN, M_xU_y (x:y=3:1, 1:1, 1:2, 1:3, 1:4) and (b) mKCN (m=1, 5, 10, 20, 40, 100 and 200) .

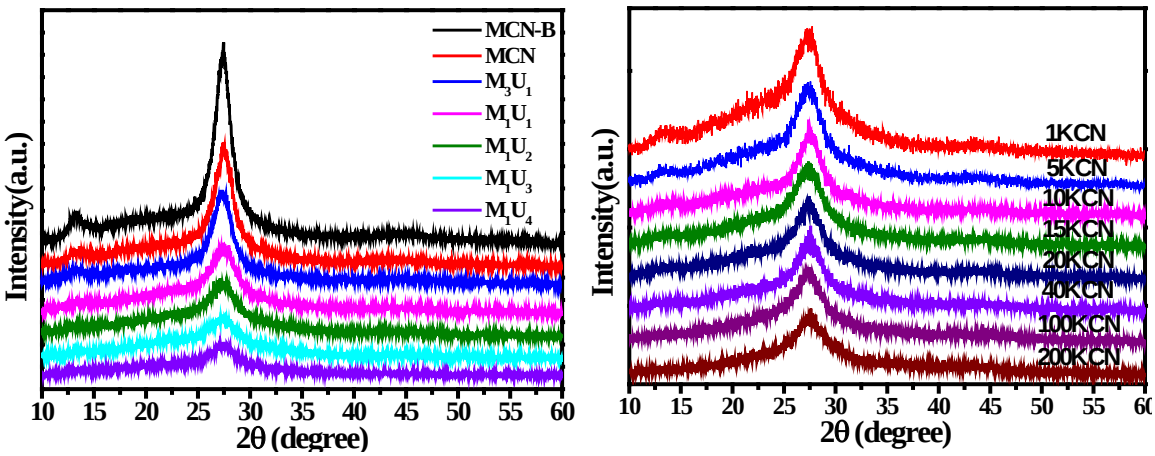

Figure S7. FTIR spectra of (a) MCN-B, MCN, M_xU_y, (b) MCN-B, 1KMCN, 5KMCN, 10KMCN, 15KMCN, 20KMCN, 100KMCN, (c) M_1U_3, 1KCN, 5KCN, 10KCN, 15KCN, 20KCN, 40KCN.

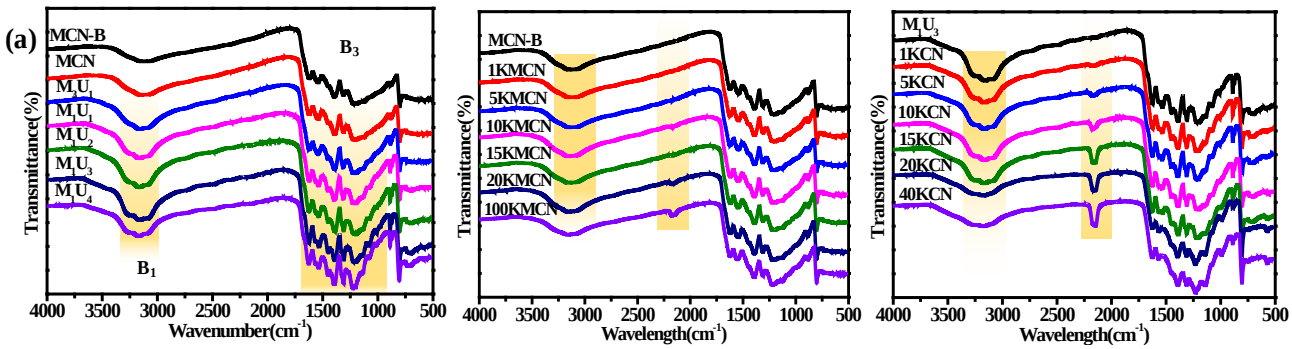

Table S2. The areas of ^{13}C MAS NMR spectra peaks centered at two binding energies from MCN-B, MCN, M_1U_3, 10KCN and 200KCN, and the peak intensity ratios of C_{3N} to $C_{2N\text{-}NHx}$ for the five samples.

Sample	$C_{2N\text{-}NHx}$	C_{3N}	C_{3N} / $C_{2N\text{-}NHx}$

MCN-B	42879.13	12534.52	0.29
MCN	42879.27	12534.68	0.29
M_1U_3	46060.3	12774.76	0.28
10KCN	24189.71	5449.93	0.23
200KCN	23142.79	3202.122	0.14

Table S3. N/C atomic ratios of MCN-B, MCN, M_1U_3, 10KCN and 200KCN measured by an organic elemental analyzer (OEA) and XPS.

Samples	**N/C (OEA)**	**N/C (XPS)**
MCN-B	1.522	1.511
MCN	1.524	1.507
M_1U_3	1.522	1.495
10KCN	1.489	1.407
200KCN	1.452	1.292

Table S4.The binding energies of the three components of C1s XPS spectrum for MCN-B, MCN, 10KMCN-B, 10KMCN, M_1U_3, M_1U_3-B, 10KCN-B, 10KCN and 200KCN, respectively, and the surface C-NH_X/C_{C1s} (the total peak area of C1s) atom ratios of the samples determined from quantitative analyses.

Sample	**C-C**	**C-NH_X**	**N=C-N**	**C-NH_X/C_{C1s}**

MCN-B	284.8	286.3	288.3	0.033
MCN	284.8	286.3	288.3	0.037
10KMCN-B	284.8	286.3	288.3	0.043
10KMCN	284.8	286.3	288.2	0.045
M_1U_3-B	284.8	286.2	288.2	0.036
M_1U_3	284.7	286.2	288.2	0.035
10KCN-B	284.7	286.3	288.2	0.044
10KCN	284.8	286.3	288.2	0.048
200KCN	284.8	286.3	288.2	0.116

Table S5. The binding energies of the three components of N1s XPS spectra for MCN-B, MCN, 10KMCN-B, 10KMCN, M_1U_3, M_1U_3-B, 10KCN-B, 10KCN and 200KCN, respectively, and the atom contents of the three nitrogen species determined from the ratios of peak areas.

Sample	**N_{2c}**	**NC_3**	**NH_X**	**N_{2c}/N_{N1s}**	**N_{3c}/N_{N1s}**	**NH_X/N_{N1s}**
MCN-B	398.7	400.2	401.2	0.744	0.188	0.068
MCN	398.7	400.2	401.2	0.741	0.188	0.071
10KMCN-B	398.7	399.8	401.2	0.630	0.300	0.069
10KMCN	398.6	399.7	401.2	0.629	0.301	0.053
M_1U_3-B	398.7	400.2	401.2	0.747	0.199	0.055
M_1U_3	398.6	400.1	401.2	0.743	0.206	0.050
10KCN-B	398.6	399.7	401.2	0.611	0.344	0.045
10KCN	398.7	399.5	401.2	0.587	0.363	0.050
200KCN	398.5	399.3	401.1	0.548	0.387	0.065

Figure S8. High-resolution XPS spectra of (a) C1s and (b) N1s in MCN-B, MCN,10KMCN-B, 10KMCN, M_1U_3-B, M_1U_3, 10KCN-B and 10KCN.

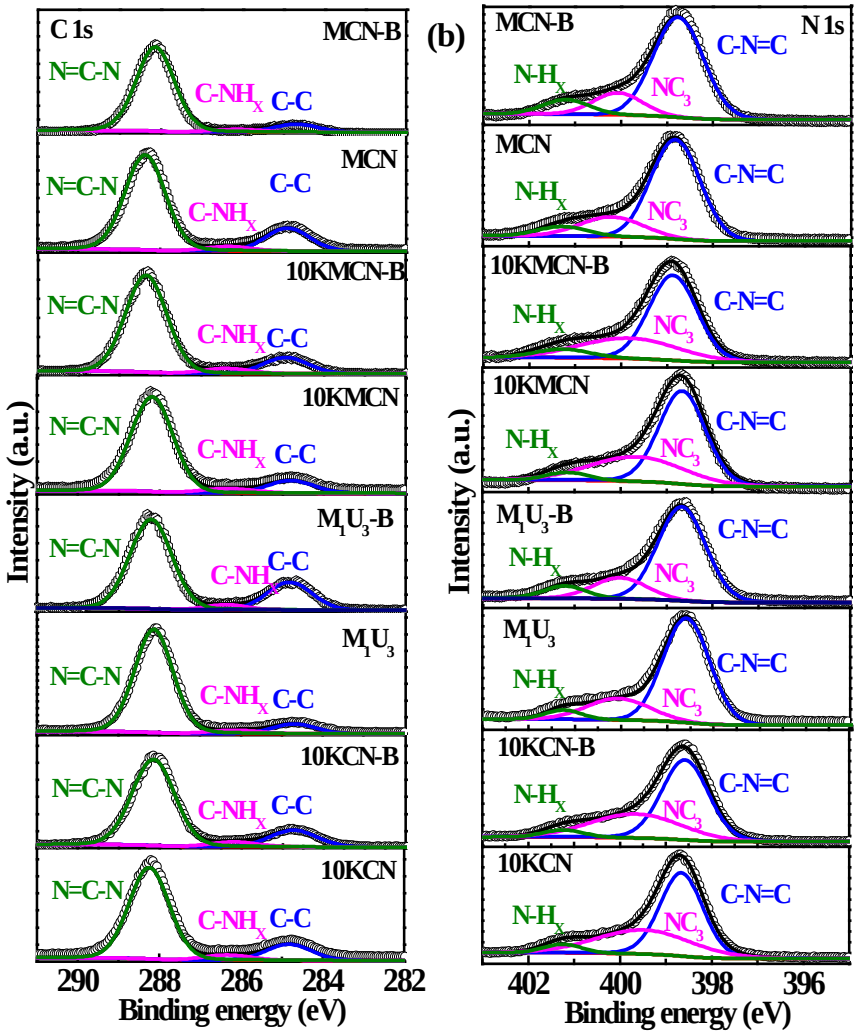

Figure S9. (a, b, c) UV-vis diffuse reflectance spectra and (d, e, f) plots of $(\alpha h\nu)^{1/2}$ versus Eg (eV) for MCN-B, MCN, M_xU_y (x:y=3:1, 1:1, 1:2, 1:3, 1:4) , mKCN (m=1, 5, 10, 20, 40, 100 and 200) and mKMCN (m=10, 20, 40, 100 and 200), respectively.

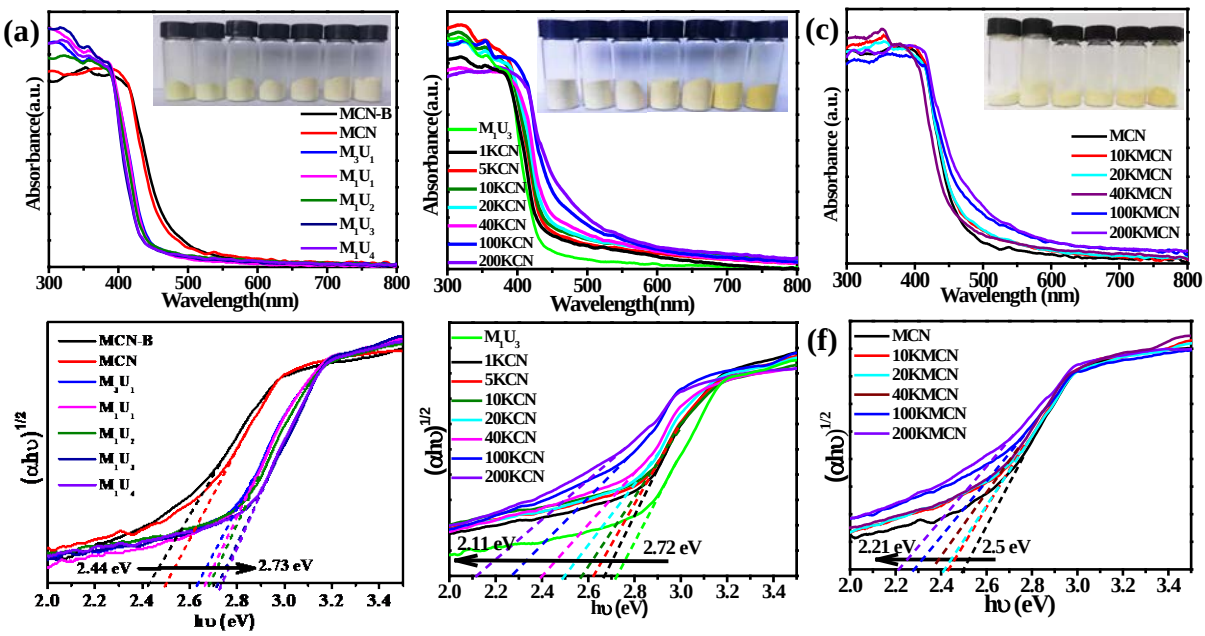

Figure S10. (a) VB-XPS spectra and (b) band structures of MCN-B, MCN, 10KMCN, M_1U_3, 10KCN and 200KCN.

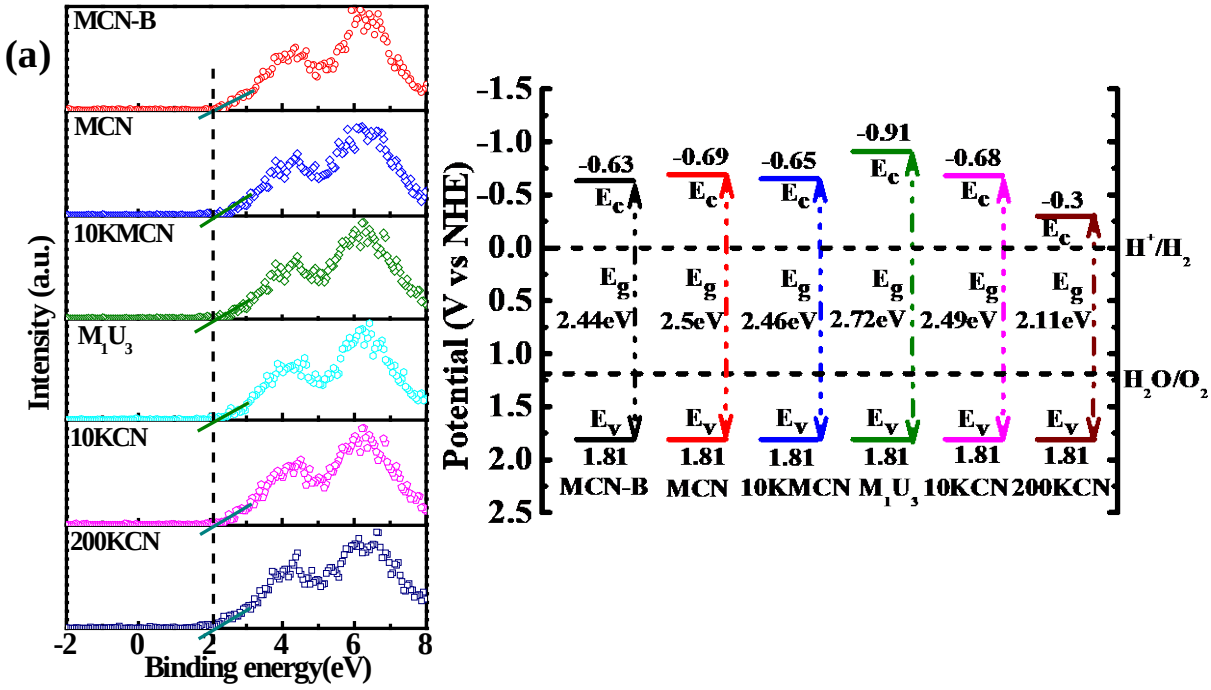

Figure S11. Structure models (a, d), calculated band structures (b, e) and corresponding DOS (c, f) of g-C_3N_4 with cyano group and N vacancy, respectively.

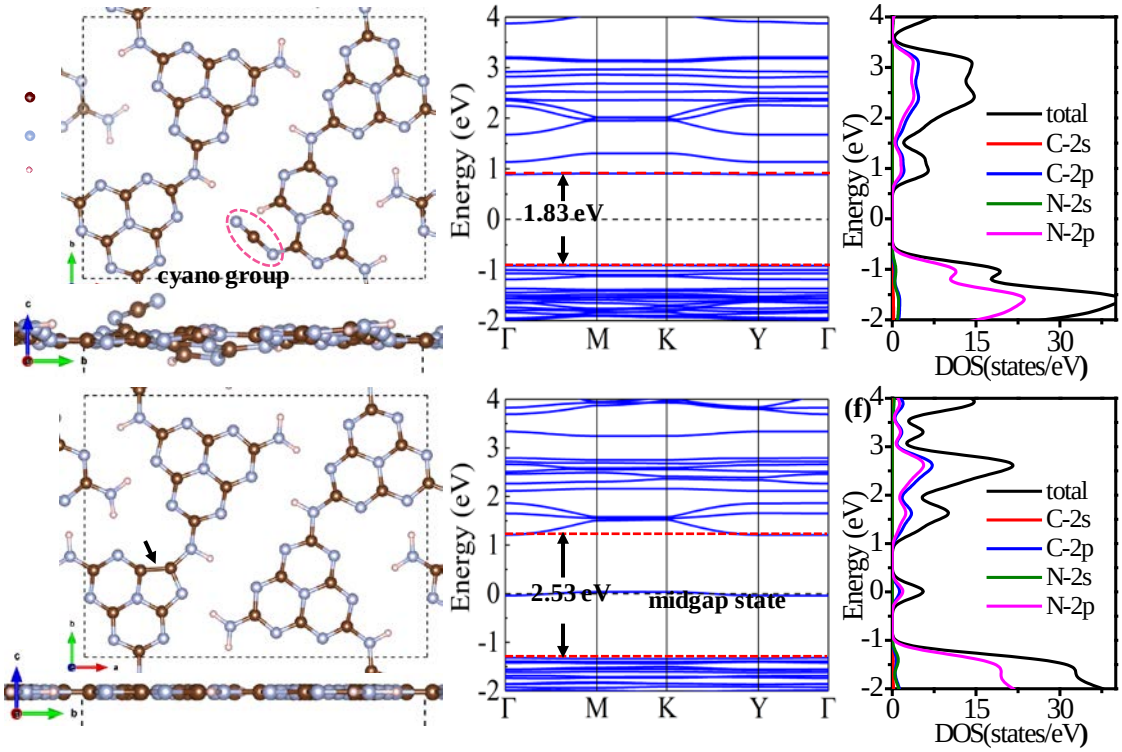

Figure S12. Photoluminescence spectra of MCN-B, MCN, M_xU_y (x:y=3:1, 1:1, 1:2, 1:3, 1:4) (a) and mKCN (m=1, 5, 10, 15, 20, 40, 100 and 200) (b), respectively.

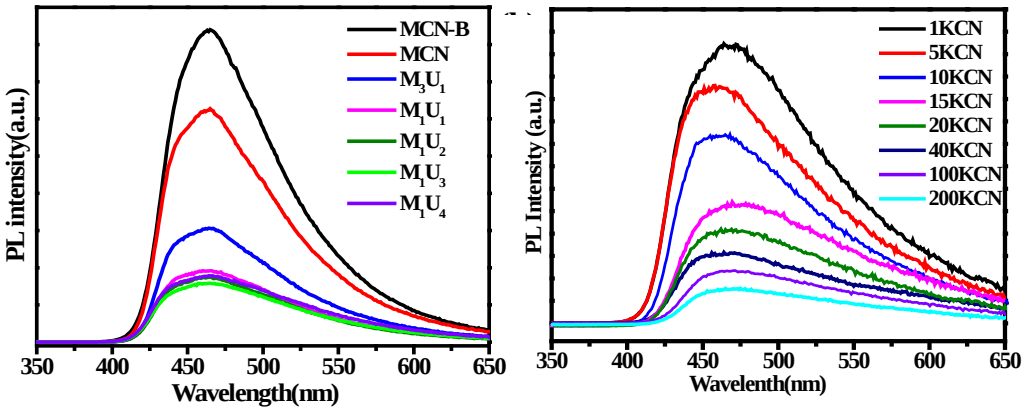

Figure S13. Time-resolved fluorescence spectra for MCN-B, MCN, M_1U_3, M_1U_4, 10KCN, 10KMCN and 200KCN.

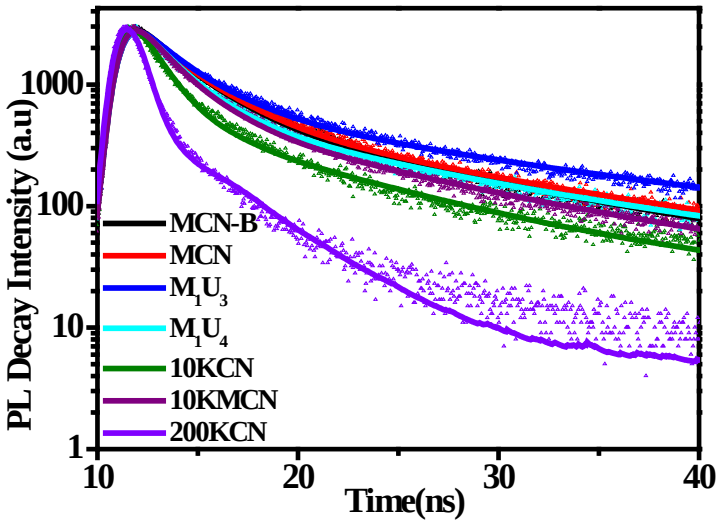

Table S6. The photoluminescence decay time (τ) and their relative amplitude (A_i) in MCN-B, MCN, M_1U_3, M_1U_4, 10KCN, 10KMCN and 200KCN, which are derived from the time-resolved PL spectra in Figure S11 by bi-exponential decays.

Sample	*i*	A_i (%)	τ_i (ns)	τ_{ave} (ns)
MCN-B	1	51.763	2.27	9.657
	2	48.237	11.256	
MCN	1	51.583	2.408	10.425
	2	48.417	12.122	
M_1U_3	1	44.405	2.331	12.440
	2	55.595	13.804	
M_1U_4	1	51.455	1.95	10.059
	2	48.545	11.515	
10KMCN	1	53.76	1.859	8.956
	2	46.24	10.427	
10KCN	1	56.805	1.3	7.690
	2	43.195	8.915	
200KCN	1	69.598	0.456	3.191
	2	30.402	3.919	

The average lifetime was calculated following the equation: $\tau_{ave} = \sum A_i \tau_i^2 / \sum A_i \tau_i$

Figure S14. Electrochemical impedance spectra in 0.1 mol L^{-1} Na_2SO_4 solution of MCN-B, MCN, M_1U_3, 10KCN and10KMCN under visible-light illumination (λ > 420 nm).

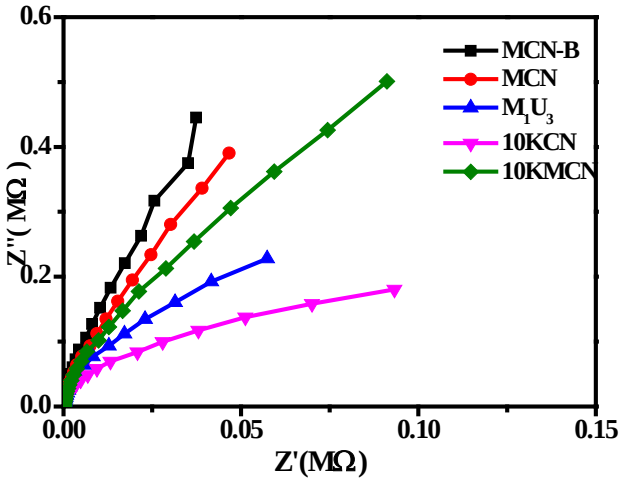

Figure S15. H_2 evolution curves of MCN-B, MCN, M_1U_3, 10KCN and 10KMCN under (a) solar light and (b) visible light irradiation (λ>420 nm), respectively.

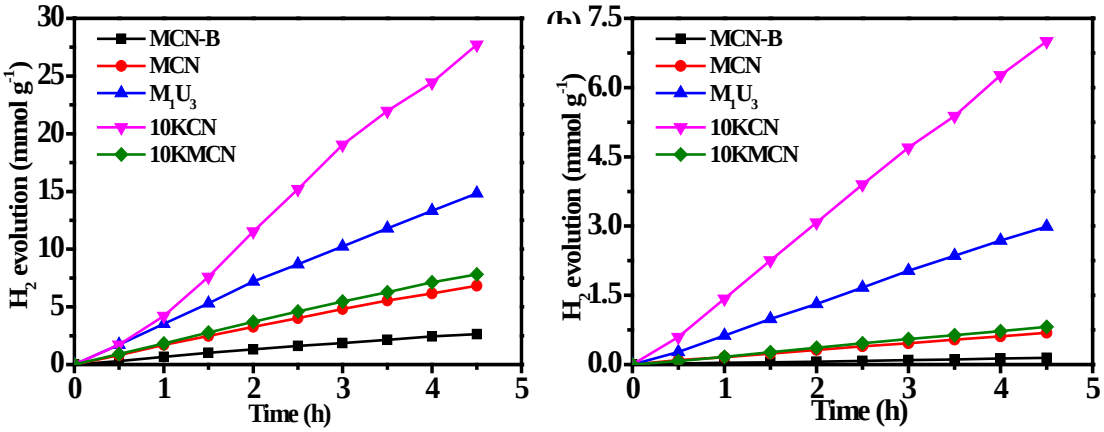

Figure S16. Photocatalytic activity of samples. (a) Photocatalytic H_2 evolution rates and (b) H_2 evolution curves of MCN-B, MCN, and M_xU_y (x:y=3:1, 1:1, 1:2, 1:3, 1:4) under visible-

light irradiation (λ > 420 nm). (c) Photocatalytic H_2 evolution rates and (d) H_2 evolution curves of mKCN (m=1, 5, 10, 15, 20, 40, 100 and 200) under visible-light irradiation (λ > 420 nm).

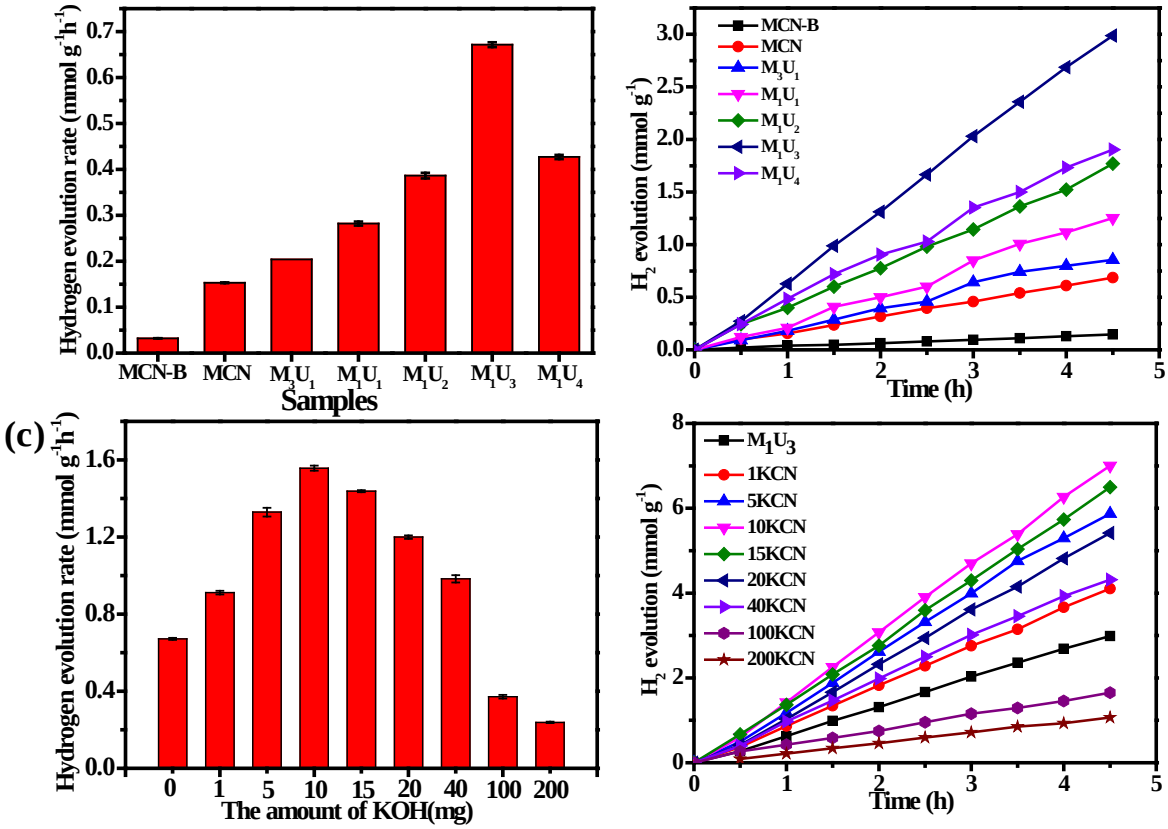

Figure S17. Typical GC chromatogram of H_2 for the photocatalytic H_2 evolution measurements (a) without TEOA, (b) without Pt and (c) with TEOA and Pt, respectively. (d)

Photocatalytic H_2 evolution curves of 10KCN and 10KCN without TEOA or Pt under visible-light irradiation (λ > 420 nm).

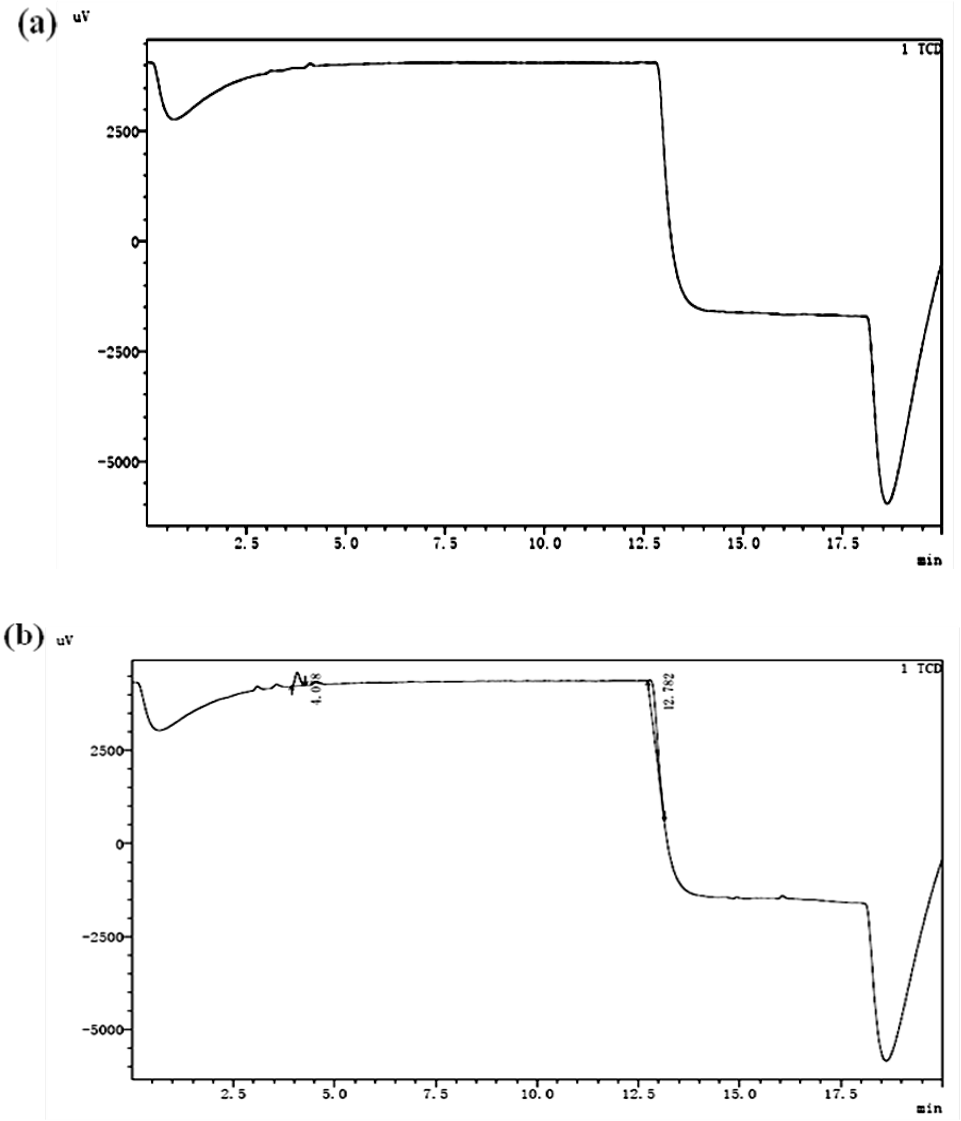

(c)

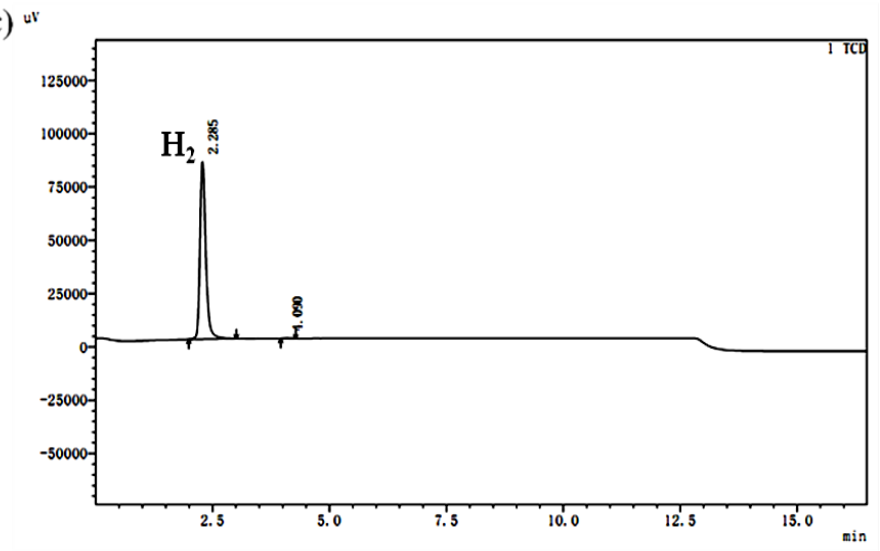
uV
1 TCD
125000
100000
75000
50000
25000
0
-25000
-50000
H2
2.285
1.090
2.5
5.0
7.5
10.0
12.5
15.0
min

(d)

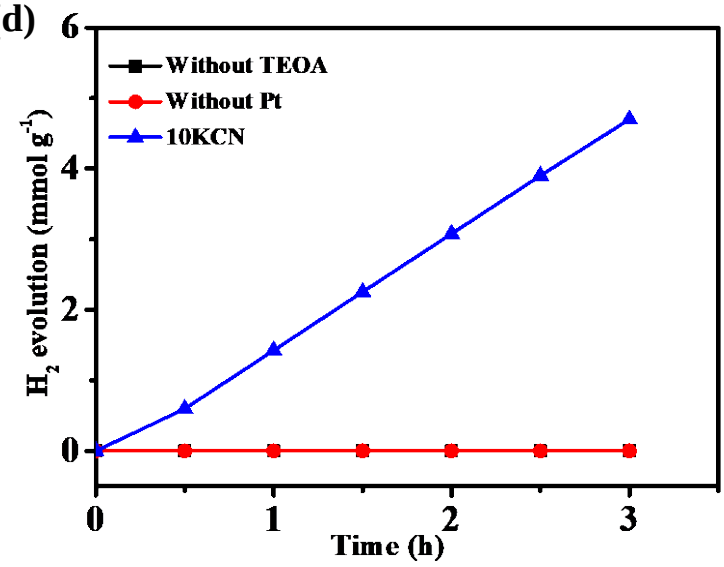
Without TEOA
Without Pt
10KCN
H2 evolution (mmol g-1)
Time (h)
0
2
4
6
0
1
2
3

Table S7. Photocatalytic activity of the 10KCN compared with the previous reported g-C_3N_4. (N-A and - means not applicable and unascertained, respectively.)

Catalysts	reaction conditions	H_2 evolution rate (μmol/$h^{-1}g^{-1}$)	The promotion of photocatalytic activity (times)	AQY (at 420/500nm)	Ref.
d-CNS	20mg catalyst, 3wt% Pt, 300W Xe, λ>420nm, 10℃,10% TEOA	3809.6	14.5	1.75/0.67	[1]
g-C_3N_4-M_1U_2	50mg catalyst, 3wt% Pt, 300W Xe,λ>400nm,room temperature, 20% TEOA	3100	3.7	28/N-A	[2]
PCN-S	50mg catalyst, 3wt% Pt, 300W Xe, λ>400nm, ambient temperature, 20% TEOA	1596	14.7	3.56/0.38	[3]
CNPS-NH_2	30mg catalyst, 3wt% Pt, 300W Xe, λ>420nm, ambient temperature, 3% TEOA	3761	6.45	-/N-A	[4]
CNK-OH	50mg catalyst, 2wt% Pt, 300W Xe, λ>420nm, ambient temperature, 10% TEOA and 0.2 mol K_2HPO_4	1370	8.5	46/N-A	[5]
CCNNSs	50mg catalyst, 3wt% Pt, 300W Xe, λ>420nm, room temperature, 10% MeOH	1060	66.2	8.57/N-A	[6]
COC30	50mg catalyst, 3wt% Pt, 300W Xe, λ>420nm, 10% TEOA	1340	4.65	8.43/0.37	[7]
CN-10	50mg catalyst, 3wt% Pt, 300W Xe, λ>400nm, 25% lactic acid	459	5.2	2.2/N-A	[8]
P-TCN	100mg catalyst, 1wt% Pt, 300W Xe, λ>420nm, 15℃, 10% TEOA	670	7	5.68/ N-A	[9]
p-CN_2	50mg catalyst, 3wt% Pt, 300W Xe, λ>420nm, 20% TEOA	395.96	6	0.79/0.05	[10]
g-C_3N_4 nanotubes	10mg catalyst, 3wt% Pt, 300W Xe, λ>400nm, 10% TEOA	11850	12.8	6.8/-	[11]

P-DCN	10mg catalyst, 3wt% Pt, 300W Xe, λ>420nm, 15℃, 10% TEOA	2092	26	1.46/-	[12]
Few-layered g-C_3N_4	10mg catalyst, 3wt% Pt, 300W Xe, λ>420nm, 5℃, 10% TEOA	1391	2.6	6.6/-	[13]
10KCN	**50mg catalyst, 3wt% Pt, 500W Xe, λ>420nm, 5℃, 20% TEOA**	**1557.7**	**48.51**	**11.2/0.85**	**This work**

Figure S18. TEM micrograph of 10KCN before (a) and after (b) loading with 3wt % Pt. (c) High resolution TEM micrograph of Pt/10KCN. (d) High Angle annular dark field image-scanning TEM (HAADF-STEM) micrograph of Pt/10KCN and the corresponding EDS elemental mapping images of C, N, and Pt elements. (e) TEM micrograph of 10KCN after photocatalytic reaction.

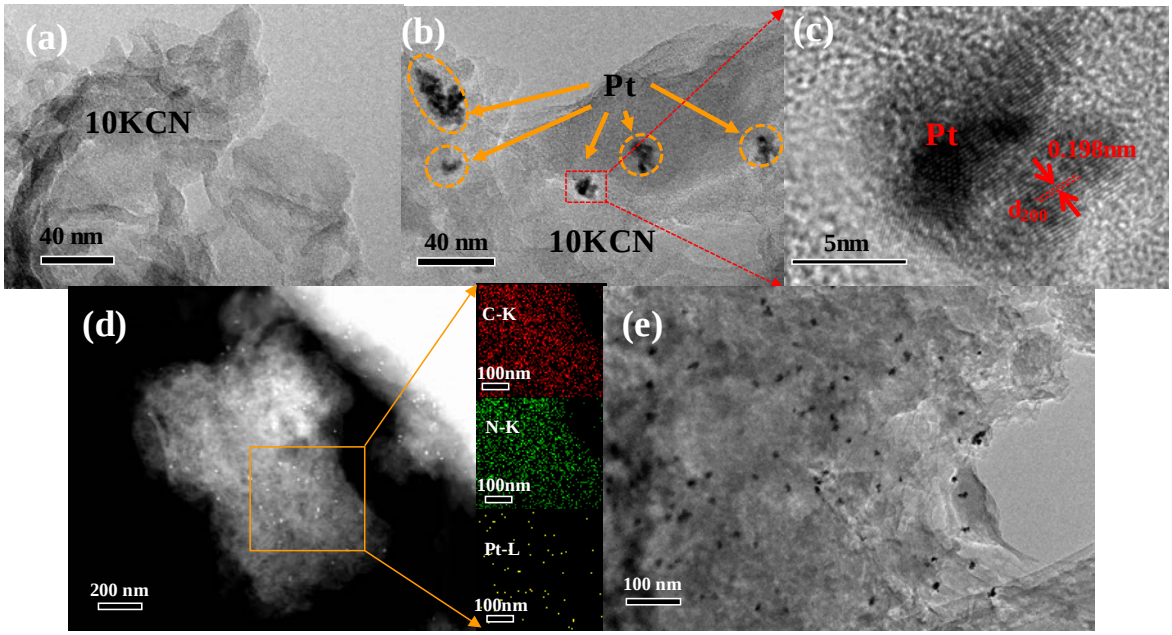

Figure S19. Characterizations of 10KCN before and after photocatalytic reaction. (a) XRD patterns and (b) FTIR spectra of 10KCN.

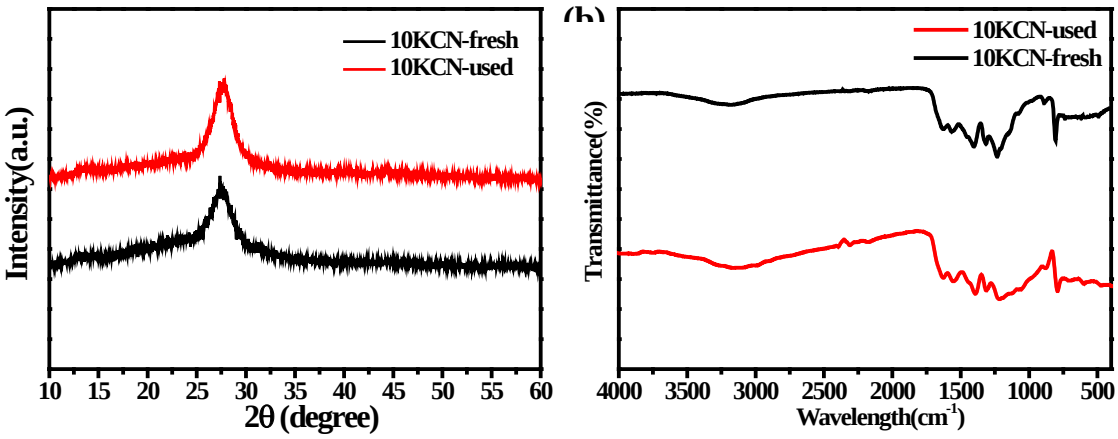

Figure S20. (a) LC/MS chromatographic profiles of the peak fraction in the aqueous solution of the reactant (triethanolamine (TEOA) was used as the sacrificial reagent), and the inset is the enlarged image of the sample with the mass range in 100~110 (105.1 and 150.1 mass can match well with DEOA and TEOA, respectively); (b) HPLC results of DEOA at intervals from the aqueous solution of the reactant.

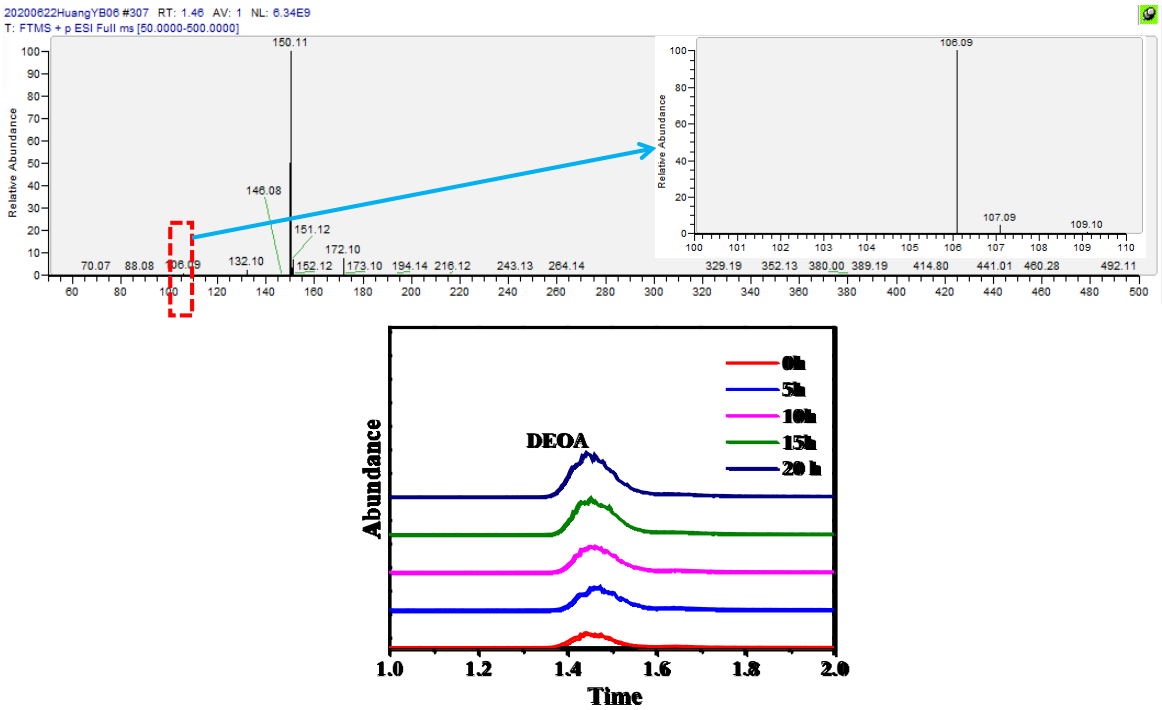

References

[1] Y. Wang, P. Du, H. Pan, L. Fu, Y. Zhang, J. Chen, Y. Du, N. Tang, G. Liu, Increasing Solar Absorption of Atomically Thin 2D Carbon Nitride Sheets for Enhanced Visible-Light Photocatalysis, *Adv. Mater.* **2019**, 31, 1807540.

[2] D. Ruan, S. Kim, M. Fujitsuka, T. Majima, Defects rich g-C_3N_4 with mesoporous structure for efficient photocatalytic H_2 production under visible light irradiation, *Appl. Catal., B* **2018**, 238, 638-646.

[3] J. Ran, T. Y. Ma, G. Gao, X.-W. Du, S. Z. Qiao, Porous P-doped graphitic carbon nitride nanosheets for synergistically enhanced visible-light photocatalytic H_2 production, *Energ. Environ. Sci.* **2015**, 8, 3708.

[4] N. Meng, J. Ren, Y. Liu, Y. Huang, T. Petit, B. Zhang, Engineering oxygen-containing and amino groups into two-dimensional atomically-thin porous polymeric carbon nitrogen for enhanced photocatalytic hydrogen production, Energ. *Environ. Sci.* **2018**, 11, 566-571.

[5] Y. Li, S. Ouyang, H. Xu, W. Hou, M. Zhao, H. Chen, J. Ye, Targeted Exfoliation and Reassembly of Polymeric Carbon Nitride for Efficient Photocatalysis, *Adv. Funct. Mater.* **2019**, 29, 1901024.

[6] H. Ou, L. Lin, Y. Zheng, P. Yang, Y. Fang, X. Wang, Tri-s-triazine-Based Crystalline Carbon Nitride Nanosheets for an Improved Hydrogen Evolution, *Adv. Mater.* **2017**, 29, 1700008.

[7] C. Yang, Z. Xue, J. Qin, M. Sawangphruk, X. Zhang, R. Liu, Heterogeneous structural defects to prompt charge shuttle in g-C_3N_4 plane for boosting visible-light photocatalytic activity, *Appl. Catal., B* **2019**, 259, 118094.

[8] F. Yang, D. Liu, Y. Li, L. Cheng, J. Ye, Salt-template-assisted construction of honeycomb-like structured g-C_3N_4 with tunable band structure for enhanced photocatalytic H2 production, *Appl. Catal.*, B **2019**, 240, 64-71.

[9] S. Guo, Z. Deng, M. Li, B. Jiang, C. Tian, Q. Pan, H. Fu, Phosphorus-Doped Carbon Nitride Tubes with a Layered Micro-nanostructure for Enhanced Visible-Light Photocatalytic Hydrogen Evolution, *Angew. Chem. Int. Ed.* **2016**, 55, 1830-1834.

[10] Y. Jiang, Z. Sun, C. Tang, Y. Zhou, L. Zeng, L. Huang, Enhancement of photocatalytic hydrogen evolution activity of porous oxygen doped g-C_3N_4 with nitrogen defects induced by changing electron transition, *Appl. Catal., B* **2019**, 240, 30-38.

[11] Z. Mo, H. Xu, Z. Chen, X. She, Y. Song, J. Wu, P. Yan, L. Xu, Y. Lei, S. Yuan, H. Li, Self-assembled synthesis of defect-engineered graphitic carbon nitride nanotubes for efficient conversion of solar energy*Appl. Catal., B* 2018, 225, 154-161.

[12] D. Zhang, Y. Guo, Z. Zhao, Porous defect-modified graphitic carbon nitride via a facile one-step approach with significantly enhanced photocatalytic hydrogen evolution under visible light irradiation, *Appl. Catal., B* 2018, 226, 1-9.

[13] Y. Hong, E. Liu, J. Shi, X. Lin, L. Sheng, M. Zhang, L. Wang, J. Chen, A direct one-step synthesis of ultrathin g-C_3N_4 nanosheets from thiourea for boosting solar photocatalytic H_2 evolution, *Int. J. of Hydrogen Energ.* 2019, 44, 7194-7204.